



Catalytic Supercritical Water Gasification of Empty Palm Fruit Bunches Using ZnO-Doped Ni–CaO Catalyst for Hydrogen Production

Y. H. Taufiq-Yap^{1,2} · S. Sivasangar^{1,2,3} · M. Surahim^{1,2}

Published online: 29 August 2019
© Springer Science+Business Media, LLC, part of Springer Nature 2019

Abstract

Supercritical water gasification (SCWG) of empty palm fruit bunches (EFBs) was investigated using ZnO-doped Ni–CaO catalysts for hydrogen-rich product gas. The catalysts were prepared via wet impregnation technique and characterized using XRD, BET, TPR–H₂, and TPD–CO₂. SCWG reactions were carried out 0.3 g of EFBs added to 5 wt% of the catalyst in 8 mL of deionized at 380 °C and the product gases were analyzed using gas chromatography. Incorporation of ZnO and Ni into CaO was found to be very active in promoting the water gas shift (WGS). From the various concentrations of dopants, 5 wt% ZnO with 5 wt% Ni was found to be the optimum loading on CaO, showing the highest hydrogen production (105.7 mmol mL⁻¹). Besides, the formation of a Ni_{0.8}Zn_{0.2}O phase from the strong interaction between the dopants was found to be an active phase in promoting the WGS reaction.

Keywords CaO · EFB · Biomass · ZnO · Water gas shift reaction

Introduction

Supercritical water gasification (SCWG) is gaining notable attention from researchers as a promising method for converting biomass into hydrogen-rich product gases. The technique is considered economical in terms of low reaction temperatures and the fact that it can tolerate high moisture contents in the feedstock, where drying is a must for current conventional thermochemical methods in use (gasification, pyrolysis, and combustion). The alternative SCWG method will have a broad application in the near future if the biomass

contains significant amounts of moisture, which would normally require prior drying before further upgrading processes.

Lignocellulose constitutes a major part of the cell wall of terrestrial plants and covers approximately 90% of accessible biomass. Tapping these huge resources in the form of agricultural, forestall, industrial residues, and wastes for second-generation biofuel is considered additional advantage where it is not in direct competition with food and feed production [1]. Palm oil industry accountable for 85.5% total biomass wastes produced in Malaysia with an average of 50 million tons dry oil palm residues annually and predicted to reach 100 million tons by 2020 [2, 3]. Among the palm oil mill wastes, empty fruit bunches (EFBs) are considered a potential feedstock for the SCWG process, due to its high moisture content and abundance, which causes waste-management problems. Even though many plausible ways have been implemented to deal with this discarded mill waste, including utilizing it as an organic fertilizer and boiler fuel, it is still not fully converted into valuable end products. Thus, EFB utilization as a SCWG feedstock is very promising and could initiate further studies in the near future on a larger scale.

The reaction temperature and the catalysts employed are the most vital factors in the SCWG that significantly impact the overall process efficiency and desired product yield. The reaction temperature of the SCWG has been classified into two main categories: low temperature (350–600 °C), which

✉ Y. H. Taufiq-Yap
taufiq@upm.edu.my

✉ S. Sivasangar
sivasangar@upm.edu.my

¹ Catalysis Science and Technology Research Centre, Universiti Putra Malaysia (UPM), 43400 Serdang, Selangor, Malaysia

² Department of Chemistry, Faculty of Science, Universiti Putra Malaysia (UPM), 43400 Serdang, Selangor, Malaysia

³ Department of Basic Science and Engineering, Faculty of Agriculture, Science and Technology, Universiti Putra Malaysia, Nyabau Road, 97000 Bintulu, Malaysia

requires catalyst addition, and high temperature (500–750 °C), which is performed in the absence of a catalyst or with a nonmetallic catalyst [4]. The types of catalysts used in SCWG reactions are categorized into heterogeneous and homogenous, based on the phase of the catalyst and the reactant. Generally, homogenous catalysts include alkaline-metal catalysts such as Na_2CO_3 , K_2CO_3 , KHCO_3 , NaOH , KOH , and $\text{Ca}(\text{OH})_2$, which are widely reported; these catalysts dissolve in water and are capable of enhancing water gas shift (WGS) reactions [5–9]. However, catalyst recovery is difficult to accomplish from the reaction phase and continued additions without recycling are expensive [5, 10]. Thus, more attention is given to the development of heterogeneous catalysts in order to achieve similar catalytic activity and high selectivity towards hydrogen production.

Numerous types of heterogeneous catalysts have been investigated to accelerate the SCWG reaction, and Azadi et al. [11] classified the catalysts into three major categories: activated carbon (AC), transition metals (supported and unsupported), and oxides. AC catalysts have been reported to actively improve WGS reactions and methanation, and almost complete carbon conversion can be achieved at reaction temperatures around 600 °C [12]. However, at lower reaction temperatures, carbon-based catalysts have been found to be inactive in improving the rate of gasification [13]. Thus, the choice of the catalyst has been expanded to a wide range of transition metals that are divided into supported and unsupported catalysts. Among the transition metals, nickel and ruthenium are widely used, owing to a promotional effect on hydrogen yield and carbon gasification [13–15]. In addition, several types of oxides have also been studied in the SCWG reaction and have shown significant improvements in hydrogen yield. Cao et al. studied the catalytic properties of 12 types of transition metal oxides (V_2O_5 , Cr_2O_3 , MnO_2 , Fe_2O_3 , Co_2O_3 , CuO , ZnO , ZrO_2 , MoO_3 , SnO_2 , WO_3 , and CeO_2) in SCWG and concluded that most of the metal oxides significantly improve the gasification efficiency and also influence the overall product gas composition [16]. Besides, CaO also has been reported to catalyze gasification reactions, hydrocarbon-reforming reactions, and WGS reactions [17]. Thus, in this investigation, CaO -based catalysts were synthesized with the addition of suitable dopants (Ni and Zn) to enhance the gasification and hydrogen-favored reaction at moderate temperature (380 °C) using EFBs as a feedstock. Based on our previous studies, the addition of Zn into Ni-doped CaO catalysts significantly improves the hydrogen yield, owing to the major promotional effect on the WGS reaction. Thus, an optimization of Zn and Ni addition into CaO catalysts was carried out and the impact on EFB gasification to produce hydrogen-rich product gas is reported.

Experimental Section

Raw Materials and Reactants

The EFB feedstock used in this study was obtained from a local palm oil processing mill at Johor, Malaysia. The raw bunch was cut into smaller pieces and dried for 2 weeks. The dried sample was ground into powder (250 μm). The weight percentages of C, H, and O in the feedstock were assessed using elemental analysis and are listed in Table 1. The chemicals that were used in the preparation of the catalysts were CaO (24856-8), $\text{Ni}(\text{NO}_3)_2 \cdot 6\text{H}_2\text{O}$ (244074), and $\text{Zn}(\text{NO}_3)_2 \cdot 6\text{H}_2\text{O}$ (228737), all purchased from Sigma Aldrich.

Catalyst Preparation

Ni- and Zn-doped CaO catalysts were prepared in a single-step wet impregnation method. The addition of dopants was fixed in the order of 5% Ni with 5, 10, and 15 wt% Zn as well as 5% Zn with 5, 8, 10, 12, and 15 wt% Ni on CaO . The aqueous solutions of metal nitrates containing pre-defined ratios were added to bulk CaO and stirred for 6 h at ambient temperature. Then, the slurries were dried in an oven at 110 °C overnight and the obtained solids were crushed into powders. The powdered catalyst precursors were calcined in air at 900 °C with a heating rate of 20 °C min^{-1} for 6 h. Then, the obtained catalysts were crushed into a fine powder and reduced at 700 °C in a partial hydrogen flow (5% H_2 -balanced Ar) 20 mL min^{-1} for 3 h. The prepared catalysts are known as 5Zn5Ni- CaO , 10Zn5Ni- CaO , 15Zn5Ni- CaO , 5Zn8Ni- CaO , 5Zn10Ni- CaO , 5Zn12Ni- CaO , and 5Zn15Ni- CaO , which were kept in a vacuum desiccator before the catalytic reactions.

Characterization

The physicochemical properties of the catalysts were characterized by X-ray diffraction (XRD), Brunner–Emmet–Teller (BET) surface area measurements, and temperature-programmed reduction (TPR). The XRD patterns of the catalysts were analyzed at ambient temperature using a Shimadzu diffractometer (model XRD6000) equipped with a Philips glass diffraction X-ray tube of broad focus 2.7 kW type to produce Cu K_α radiation. The BET surface areas of the catalysts were obtained using a Thermo Finnigan Sorptomatic 1900 series instrument via N_2 adsorption/desorption isotherms patterns at -196 °C. TPR analysis was performed using Thermo Finnigan TPDRO 1100 apparatus equipped with a thermal conductivity detector. Each sample (20 mg) was pretreated in a N_2 environment and continued analysis was performed in a 5% H_2 /argon flow (flow rate = 25 mL min^{-1}) in the temperature range 50–900 °C. TPD- CO_2 measurements performed with catalyst (20 mg) pretreatments at 400 °C in a

Table 1 Physicochemical properties of the prepared catalysts

Sample	BET surface area (m ² g ⁻¹)	Pore volume (cm ³ g ⁻¹)	CaO crystallite size (nm)	Ni crystallite size (nm)
5ZnO/5Ni–CaO	2.9	0.0098	50.40	–
10ZnO/5Ni–CaO	3.0	0.0083	41.60	–
15ZnO/5Ni–CaO	3.6	0.0100	41.10	–
5ZnO/8Ni–CaO	4.9	0.0109	38.20	39.82
5ZnO/10Ni–CaO	3.4	0.0083	57.70	32.67
5ZnO/12Ni–CaO	3.1	0.0050	51.20	29.69
5ZnO/15Ni–CaO	2.8	0.0038	57.4	34.03

N₂ flow were subjected to CO₂ gas adsorption at 50 °C for 1 h. Raising the catalyst temperature releases the adsorbates (CO₂) in the presence of a carrier gas (He), which are detected by a thermal conductivity detector (TCD).

Catalytic Reaction

A custom-made reactor system was designed (Fig. 1) using stainless-steel tubing (SS-810-6-2, outside diameter (OD) = 1/8 in) connected with one-way valves. SCWG reactions were carried out in 13-mL reactor cells made from stainless-steel tubing (SS-t8-049-6ME) with OD = 1/2 in. A Swagelok transducer (limitation 0–400 atm) was used to measure the pressure of the reactor cell during the reaction. The catalytic tests were performed using 0.3 g of the feedstock (EFB) and 5 wt% of a catalyst loaded into the reactor cell, followed by 8 mL of deionized water. The catalytic tests were replicated 3 times. A gas chromatograph (GC) oven was used as the heating chamber; the reactor cell was placed inside and the temperature was increased from 30 to 380 °C with a ramping rate of 10 °C min⁻¹. Then, the reaction time was fixed at 8 min. The reactor was cooled after the completion of each reaction, and both valves were opened intermittently to release the product gas, which was then trapped and collected using a 1-mL Luer lock gas-tight syringe. The gaseous products were injected

into a GC with a thermal conductivity detector (GC-TCD) equipped with Porapak Q and Mole Sieve columns for CO₂, H₂, CH₄, and CO detection.

Results and Discussion

Characterization

Crystalline structures of the calcined catalysts after reduction were examined using XRD, and the patterns are shown in Fig. 2. The obtained catalyst diffraction patterns exhibit three distinctive peaks relative to the presence of CaO at 32.4, 37.5, and 54°. In addition, several Ca(OH)₂ peaks appeared in the spectra with lower intensities at 18, 34.2, and 51.8°, as result of CaO hydration caused by moisture from the environment at ambient temperature. Furthermore, the peak corresponding to Ni was detected at 44.6°, indicating the reduction of NiO to metallic Ni after catalyst reduction. However, the presence of Ni is hard to rule out at 5 wt% loading in the XRD patterns, owing to better dispersion of Ni⁰ on the CaO surface, even with increasing ZnO addition (Fig. 2a–c). Similar observation was reported by Xia et al. (2012), where no obvious diffraction peak observed with 3 and 9 wt% of Ni loading on SiO₂ due to smaller NiO particles size which is highly dispersed on

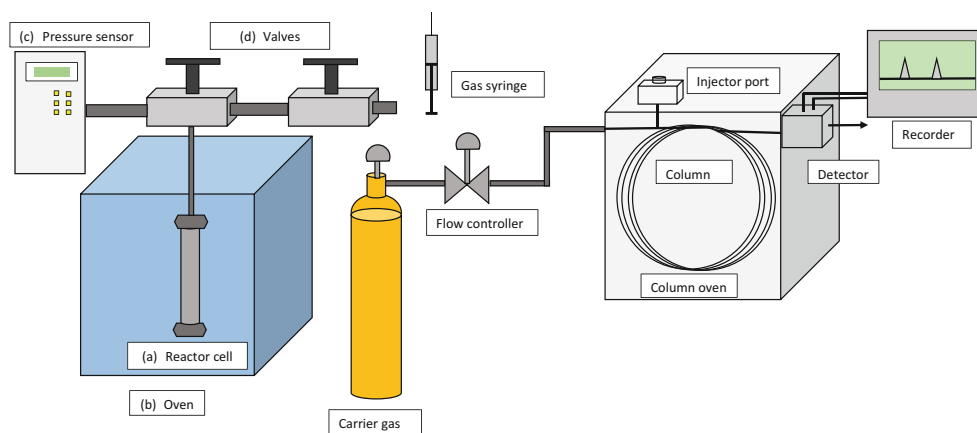
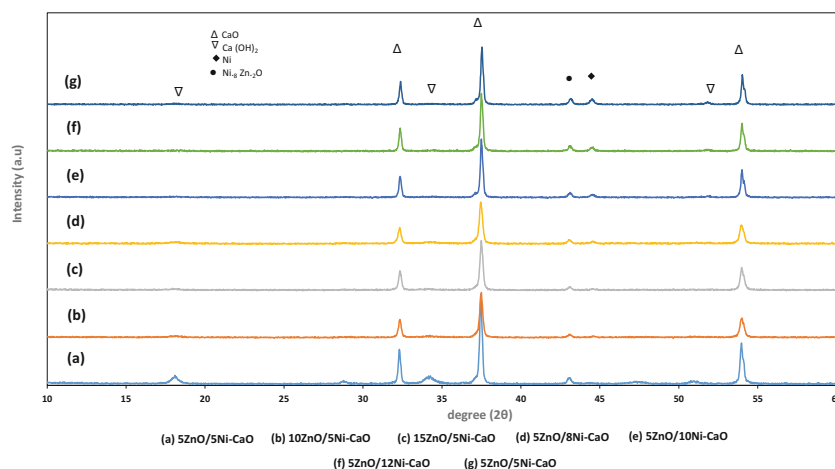
Fig. 1 Schematic diagram of the reactor

Fig. 2 XRD patterns of synthesized catalysts

the support [18]. However, the peak intensity relative to Ni was found to increase with Ni loading, owing to possible growth in the Ni crystallites caused by weak interactions with the support. Apart from this, another obvious diffraction peak at 43.1° is possibly caused by the formation of $\text{Zn}_x\text{Ni}_{1-x}\text{O}$ phases, which could be caused by the strong interactions between NiO and ZnO on the support. Besides, the ability of larger Zn^{2+} to substitute Ni^{2+} in the NiO lattice facilitates solid solution formation, caused by the ability of Zn to dissolve into the NiO rocksalt lattice [19]. Table 1 summarizes the average CaO and Ni cluster size of the catalysts, which was calculated from the diffraction spectra and Scherrer equation. The CaO crystallite sizes vary slightly in the range of 41–57 nm, owing to the incorporation of various added dopants, which tend to create defects and alter the crystallographic structure. At a lower concentration (5 wt%), the particle sizes of Ni are difficult to calculate, caused by high dispersion on the support, as mentioned earlier based on the XRD peaks. However, the presence of metallic Ni peaks with higher loadings is caused by particle agglomeration, where the sizes are in the range of 30–40 nm. The BET surface areas of the catalysts and the pore volumes were measured using N_2 adsorption/desorption techniques and the results are presented in Table 1. Bulk CaO catalyst exhibited a small surface area ($\sim 5.5 \text{ m}^2 \text{ g}^{-1}$) and low porosity [20], and similar properties were observed with all of the prepared catalysts with the addition of ZnO and Ni on CaO. The characterized catalysts show low surface areas in the range of $2.8\text{--}4.9 \text{ m}^2 \text{ g}^{-1}$, which were affected by the added dopants.

Temperature-Programmed Desorption– CO_2 Analysis

The basicity of the catalysts and the basic site distribution were measured using TPD– CO_2 analysis. The total amounts of CO_2 desorption and the absorption strength as functions of temperature are presented in Table 2 and the TPD– CO_2 profile can be seen in Fig. 3. Table 2 shows that all of the prepared

catalysts show a basic nature as a result of CaO intervention as the support, which dominates the overall catalyst properties. However, the addition of Zn and Ni altered the basicity and the distribution of sites, where a slight variance is noted with the amount of added dopants. The basicity of the catalysts with increased Zn loading was found to increase up to 10 wt% and a minor drop occurred at a loading of 15 wt%. Ni loading in the range of 5–15 wt% into CaO that contained the same amount of ZnO shows a clear increasing trend in the catalyst basicity. However, Ni and ZnO were reported to have no significant contribution in terms of basic site increments, whereby both were considered to not have notable basic properties [21, 22]. Thus, the distortion and defects that have been created by strong interactions between the added dopants on the CaO crystals structure were responsible for changing the basicity of the prepared catalysts. Basicity was found to be increased with the incorporation of NiO into the CaO lattice due to the existence of strong basic sites that formed between the binary oxides [23].

Temperature-Programmed Reduction– H_2 Analysis

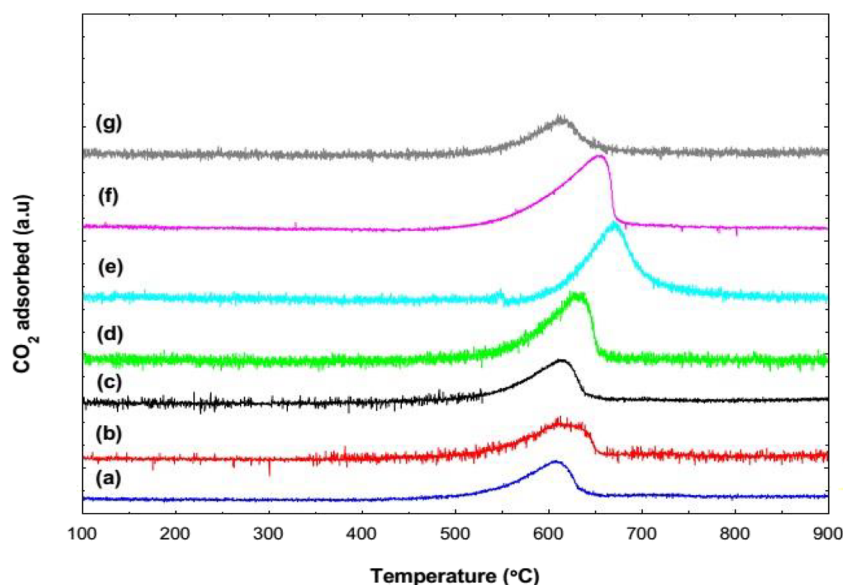
It was reported that the reduction of NiO is necessary when the presence of a Ni phase on the support was found to be active in catalyzing the SCWG reaction and elevating hydrogen production [11, 24]. Thus, all of the prepared catalysts were reduced in 5% H_2/Ar flow at 700°C for 3 h. Thus, TPR analyses were carried to study the reducibility of the catalysts, which will provide a basic understanding of the dopants interaction on the CaO surface. Reducibility of the individual components of the catalysts, including CaO, NiO, and ZnO that have also been reported previously, whereby bulk CaO and ZnO are hard to reduce, as both oxides possess very strong Ca–O and Zn–O interactions [25]. However, from our TPR analyses, we found a very small reduction peak for bulk CaO at 610.3°C , which was probably caused by a weak Ca–O bond reduction at the surface (not shown here). In addition, bulk NiO tends to

Table 2 Basicity and reducibility of the catalysts

Catalyst	CO ₂ desorbed (μmol g ⁻¹)	Peak temperature (°C)	H ₂ consumption (μmol g ⁻¹)	Peak temperature (°C)	
				Peak 1	Peak 2
5ZnO/5Ni-CaO	1315.1	609.5	410.5	561	893
10ZnO/5Ni-CaO	1612.6	620.3	443.5	583	900
15ZnO/5Ni-CaO	1598.0	613.6	481.0	579	862
5ZnO/8Ni-CaO	2296.5	632.0	842.4	581	845
5ZnO/10Ni-CaO	2360.7	672.0	1440.0	578	844
5ZnO/12Ni-CaO	2736.5	655.0	1805.8	560	840
5ZnO/15Ni-CaO	2813.5	615.3	1910.5	568	838

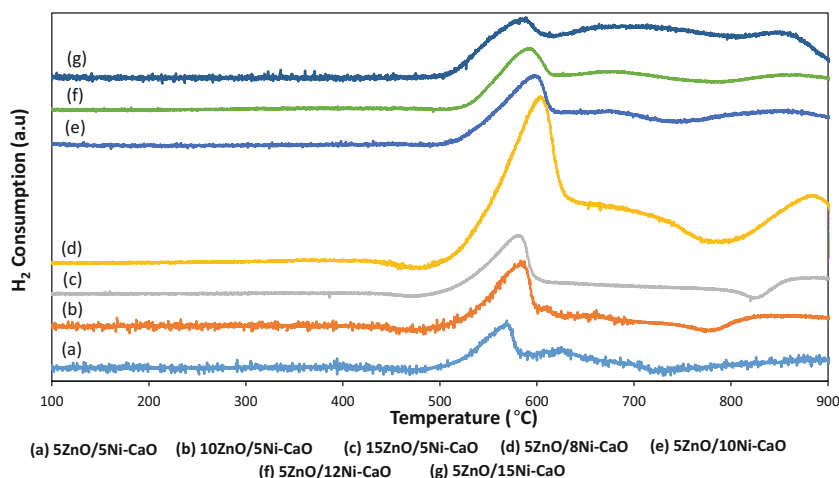
be reduced at temperatures in the range of 400–418 °C, where flowing hydrogen scavenges the lattice oxygen ($\text{NiO} + \text{H}_2 \rightarrow \text{Ni} + \text{H}_2\text{O}$) and leaves active metallic Ni on the catalyst [26]. However, the difference in the reduction temperature in the formulated catalysts compared with the bulk condition can postulate the strength of the dopant attraction on the CaO surface, which can be classified into weak (200–400 °C), medium (400–600 °C), and strong interactions (> 600 °C) based on the reduction peak occurrence relative to the temperature. The TPR profiles show that there are two distinctive peaks in the temperature range of 450–600 °C and above 700–900 °C (Fig. 4). This is attributed to the strength of the interaction of NiO on the CaO surface, as both CaO and ZnO are difficult to reduce. Addition of nickel into the CaO catalyst shows a reduction peak at 555.4 °C, which appears close to the first

temperature range. Thus, it can be concluded that the first reduction peak is caused by medium interactions between NiO and the CaO surface. However, with the addition of a secondary dopant (ZnO), a second peak appears in a higher temperature range, indicating very strong interactions between NiO and the catalysts. This is attributed to several possibilities such as new interaction establishment between NiO and the ZnO dopant or the formation of smaller NiO particles dispersed on the CaO surface, which shift the reduction temperature to the right. According to previously published reports, bulk and larger NiO particles tend to be reduced at lower temperatures compared with the smaller-sized particles that form very strong interactions with the support [27]. However, from the XRD patterns of the synthesized catalysts, the presence of a Ni₈Zn₂O phase was identified in all of the

Fig. 3 Temperature-programmed desorption–CO₂ of synthesized catalysts

a) 5ZnO/5Ni-CaO, b) 10ZnO/5Ni-CaO, c) 15ZnO/5Ni-CaO, d) 5ZnO/8Ni-CaO, e) 5ZnO/10Ni-CaO, f) 5ZnO/12Ni-CaO, g) 5ZnO/15Ni-CaO

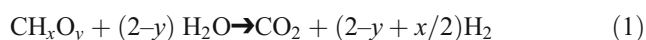
Fig. 4 Temperature-programmed reduction–H₂ of synthesized catalysts



prepared catalysts as result of strong interactions between NiO and ZnO on the support. Incorporation of the added dopants shift the reduction peak to higher temperatures, where some of the NiO remains unreduced at 700 °C under a partial hydrogen flow. Furthermore, Table 2 summarizes the reducibility of each prepared catalyst and its reduction peak relative to temperature. It was found that only slight changes in H₂ consumption were observed with increasing ZnO, owing to its non-reducible behavior and the similar NiO content on the catalysts. Besides, the appearance of a Ni₈Zn₂O peak is more visible when the reduction peaks are observed at 893, 900, and 863 °C with increasing ZnO loading. Furthermore, a higher amount of H₂ consumption was noticed in the reduction of the catalysts (Ni²⁺ → Ni⁰) with increasing Ni loading. However, the TPR profile (Fig. 4) shows that increasing the Ni loading causes a new peak to form at 650 °C, which overlaps with other reduction peaks that existed previously. Thus, swelling in the region at 600–750 °C and shifting of the second reduction peak to a lower temperature indicates the possibilities of Ni particle agglomeration at higher concentrations on the CaO. In addition, increasing the Ni loading accelerates the nucleation of larger NiO crystallites and causes the high-temperature reduction peak to shift to lower temperatures, owing to its weak interaction with the support [28].

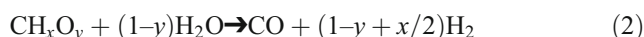
Catalytic Supercritical Water Gasification

SCWG reaction is a promising technique for biomass conversion into hydrogen-rich product gas to overcome biomass with high water content. There have been many plausible reaction mechanisms proposed in previous reports that represent the complex pathway of the reaction. However, the overall chemical conversion can be simplified as follows (Eq. (1)) [29]:



where *x* and *y* represent the elemental molar composition of H/C and O/C in biomass.

Based on the defined reaction mechanism, the overall product gas compositions from the SCWG reaction can be predicted to mainly consist of H₂ and CO₂. However, a small amount of the gas includes CO, and hydrocarbons (C₁–C₄) also tend to be produced during the reaction. Besides the summarized reaction mechanism, in reality, there are many intermediate reactions, which include steam reforming (Eq. (2)), methanation (Eq. (3)), and WGS reactions (Eq. (4)).



In addition, the reaction temperature and catalyst used in the SCWG reaction significantly influence the reaction efficiency and product gas composition. The reaction temperature has been classified into three main categories: < 374 °C (sub-critical), 374–500 °C, and > 500 °C [29]. However, water reaches a supercritical state at ≥ 374 °C, where its specific properties enhance biomass gasification to produce hydrogen-rich product gas. Catalyst are applied in order to enhance selectivity towards hydrogen and to enable biomass conversion at lower reaction temperatures. There are various types of catalysts that have been reported, such as metallic Ni-based catalyst, activated carbon, noble metals, and several oxides including ZrO₂, CaO, and CeO₂ [12, 14, 17, 24, 29–31]. Based on our preliminary studies, we found that ZnO-doped Ni–CaO catalysts significantly enhance hydrogen production during EFB SCWG at 380 °C [32]. The promotional effects of ZnO dopant on SCWG catalyst such as strong basicity and water splitting capabilities were found to be a major factor in the increment of hydrogen yield [33]. Furthermore, the synergic effect of the combination of CaO,

ZnO, and Ni leads to greater promotional effects in the WGS reaction, showing that a major source of hydrogen production in the SCWG reaction. Apart from its use as the reactant medium, the tendency of water participation in the WGS reaction represents a promising way to elevate the overall hydrogen production. Thus, the preparation of ZnO-doped Ni–CaO with different dopant loadings is essential in order to optimize the catalyst formulation to achieve higher catalytic activities.

Effect of ZnO Loading on 5 wt% Ni–CaO

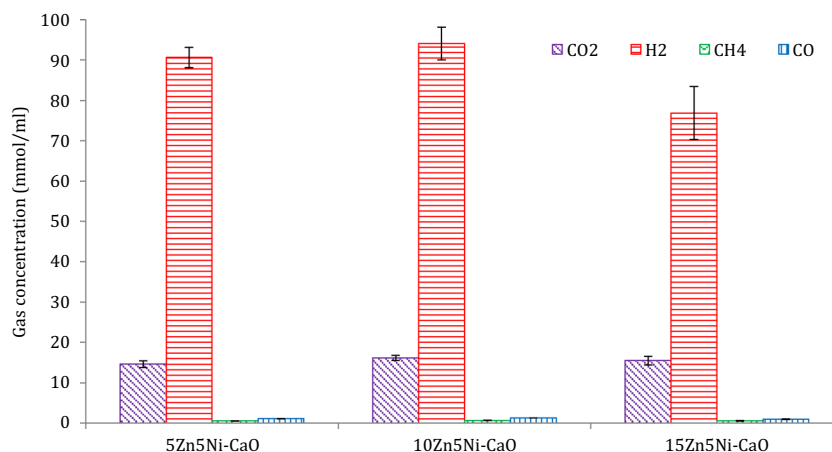
Figure 5 shows the product gas composition caused by ZnO dopant loading (5, 10, and 15 wt%) onto 5 wt% Ni–CaO catalysts during EFB SCWG at 380 °C. The gas compositions were slightly varied with catalysts, as a result of the different amount of ZnO present in the catalyst. Product gas composition shows that the major part of the gas consisted of H₂ and CO₂, whereas CO and CH₄ were measured in very low concentrations. Similar to the postulated biomass-conversion pathway, according to Eq. (1), the gases were produced from various reaction mechanisms and structural cleavages, which took place under supercritical conditions. Catalytic SCWG of EFB with increasing ZnO loading (5, 10, and 15 wt%) on Ni–CaO catalysts does not improve the hydrogen production and started to drop from 105.7 (5 wt%) to 94.1 (10 wt%) and 76.8 mmol mL⁻¹ (15 wt% loading). The main sources of hydrogen produced during SCWG are from the WGS reaction and from hydrocarbon-reforming reactions. The presence of ZnO in Ni–CaO catalyzes the WGS reaction, whereby increasing the loading beyond 5 wt% reduces the hydrogen concentration. Increasing ZnO addition shows a negative effect on the WGS reaction. This phenomenon is possibly caused by ZnO agglomeration, owing to large loading and coverage of the active sites of CaO, which are involved in the gasification reaction. Besides, the present of Ni₈Zn₂O phase on CaO initiates synergistic effects, which ease the WGS reaction. Thus, the stability of the Ni₈Zn₂O phase is

vital to promote WGS under harsh supercritical conditions. The prediction correlates with the performance of the catalysts, where the presence of a Ni₈Zn₂O peak in TPR shifts to a lower temperature with increasing ZnO loading. Besides, several previously published reports have mentioned that the presence of metallic Ni also promotes the WGS reaction along with increased carbon conversion [14, 34, 35]. However, the methanation reaction, classified as the hydrogenation of CO and CO₂ by the metallic Ni dopant, has notable drawbacks, which tend to reduce hydrogen production. Apart from this, CaO catalysts have shown significant contributions to high hydrogen production, due to its dual role as a CO₂ sorbent and as a catalyst during the EFB SCWG reaction. The potential application of CaO in SCWG was reported by Zhang et al. [17], using coal–water slurry SCWG reaction, where CaO was found to catalyze the gasification, WGS, and reforming reactions. Furthermore, the basic nature of CaO offers an additional advantage to promote the WGS, which is propelled by the cyclic coordination of intermediate anions that are involved in hydrogen production. It has been described based on carbonate conversion to formate in the presence of CO and water that form an intermediate compound (formaldehyde) which decomposes to H₂, CO, and CO₃²⁻. Subsequently, CO and CO₃²⁻ ions are used back in the reaction mechanism where CO₂ released at the end [36].

Effect of Reaction Time on ZnO-Doped 5 wt% Ni–CaO

From our experiments in the absence of a catalyst, the reaction time of EFB SCWG was found to have no effect on the product gas composition or feedstock gasification. This is attributed to the formation of thermally stable tarry compounds, which are hard to degrade at the reaction temperature. Thus, increasing reaction time shows less impact on the overall product gas composition and only a slight variation is observed in the amount of H₂ and CO, caused by the progressing WGS reaction with time. Thus, the effects of reaction time on the overall product gas

Fig. 5 Effect of ZnO loading of 5 wt% Ni–CaO on EFB SCWG reaction



composition (CO₂, H₂, CH₄, CO) in the presence of the prepared catalysts are presented in Fig. 6. The results show that notable differences in the product gas composition occurred with increasing reaction time for the added catalysts reaction. However, there are no clear patterns in CO₂ production with increasing reaction time using the added catalysts. Plausible ways to CO₂ production are mainly through carboxyl group cleavages from the biomass structures [37] or CO conversion through the WGS reaction. An almost similar CO₂ concentration shows that there is no further degradation in the dissolved biomass with increasing time or with increasing ZnO loading on the added catalysts. However, H₂ production is directly proportional to reaction time, whereby its concentration linearly increases with time. Even though the addition of catalysts altered the level of hydrogen production, a steadily increasing trend is seen with increasing reaction time. This phenomenon postulates that the progressing WGS and reforming reactions, aided by the added catalysts with increasing reaction time, elevate the overall level of hydrogen production. Among the catalysts, the 5% ZnO-doped catalyst shows steady H₂ production with increasing reaction time, in contrast to the 10 and 15% doped alternatives. This shows that increasing the ZnO

content has negative effects in terms of hydrogen-favored reactions. In conclusion, the 5% ZnO-doped catalyst was found to be promising, whereby a steady increase in hydrogen production was observed with increasing reaction time from 8 to 32 min due to progressing WGS reaction. In addition, the concentration of CH₄ shows a linear increase with reaction time. Generally, CH₄ production was linked to two factors, including functional group cleavage and methanation reaction [14, 38]. It is reported that CH₄ mainly produced from breaking of functional groups (O–CH₃) [34], where the dissolved liquid oxygenates from EFB slowly degraded in the supercritical environment [38]. Besides, numerous reports have stated that the methanation reaction is highly favored in the presence of metallic Ni catalysts [31, 39]. Even though CH₄ production is relatively low compared with H₂ and CO₂, its increment could still cause a reduction in the H₂ yield. Among the catalysts, 5% ZnO-doped catalyst shows a higher tendency for CH₄ production, which is possibly caused by well-dispersed metallic Ni on the catalyst surface without strong interactions with ZnO. Besides, the CO concentration shows a steady reduction with increasing reaction time, as a result of the advancing WGS reaction caused by the added catalysts, as

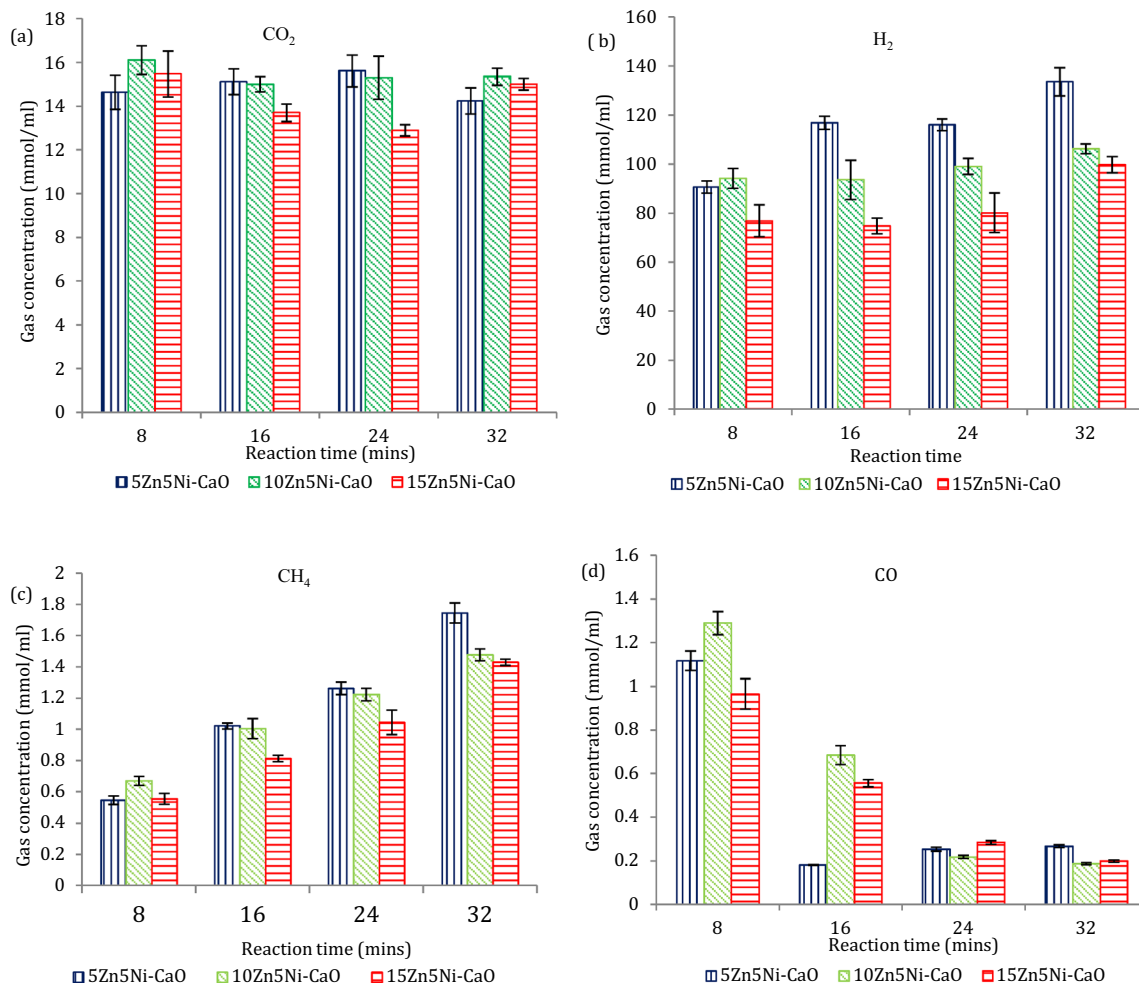


Fig. 6 a–d Effect of reaction time on the ZnO-doped 5 wt% Ni–CaO catalyst

predicted earlier. Thus, from the CO reduction patterns over time, the 5 wt% ZnO-doped catalyst caused a drastic drop at 16-min reaction time compared with other catalysts, whereas a further increase in time shows a similar concentration. It can be concluded that, among the tested catalysts, with increasing reaction time (8–32 min), the 5 wt% ZnO-doped Ni–CaO catalyst exhibits high catalytic activity towards hydrogen production. However, in terms of overall carbon concentration in the gas, the phases show similar patterns (15–18 mmol mL⁻¹) and residues are found in the reactor even after prolonging the reaction time (Table 3). This shows that complete carbon conversion is hard to achieve, even with catalyst addition, owing to lower reaction temperature (380 °C). However, the application of Ru catalyst in SCW reaction at the similar condition to the current investigation shows catalytic activity maintained with an increase in reaction time (5–15 min). In addition, carbon yield linearly improved [40] compared with 5 wt% ZnO-doped Ni–CaO catalyst where carbon gasification was stagnant with an increase in reaction time. This is possibly due to the Ni particles sintering or potential surface oxidation of Ni which lowers the catalytic activity and gas yield.

Besides, reaction temperatures in the range of 380–600 °C were considered lower temperatures for SCWG, whereby complete carbon conversions are difficult to achieve even with the addition of catalysts [4]. Generally, noble metal catalysts (Ru) are employed, which give considerable carbon conversion at lower reaction temperatures [4, 41]. However, noble metals are associated with higher catalyst costs whereby Ni-based catalysts are preferred and selected for SCWG. Despite several drawbacks such as catalyst deactivation, methanation reaction, and higher reaction temperature requirement (> 450 °C), the catalyst performance can be enhanced with the addition of dopants. Besides, the nature of EFBs also contributes to the lower carbon conversion, which is caused by its complex intrinsic components. Differences in the thermal stability of each component in EFBs dictate the overall degradation patterns and greatly influence the product gas

composition and residue formation. In comparison with EFBs, which consist of a complex structure (lignin, cellulose, and hemicellulose), model compounds are generally used to study degradation patterns in SCWG. Among the components, lignin tends to produce the highest number of residues and it is hard to gasify, aided by its strong physical structure compared with other lignocellulosic model compounds like cellulose, hemicellulose, and glucose [34]. Thus, the combination of these compounds in EFBs also influences its degradation compared with pure lignocellulosic model compounds.

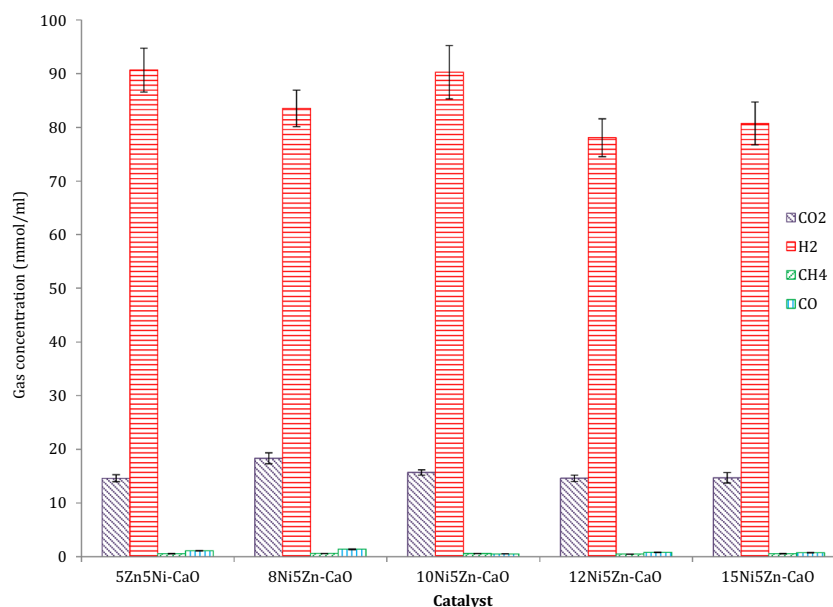
Effect of Ni Loading on 5 wt% ZnO–CaO Catalysts

Apart from ZnO loading, the effect of Ni addition (5–15 wt%) on CaO in EFB SCWG is reported in Fig. 7. The product gas composition varies slightly with increasing Ni addition to the catalysts. It was found that increasing the Ni loading (5, 8, 10, 12, 15 wt%) does not show any significant improvements in H₂ production, where a reduction in the hydrogen concentration is observed. Thus, it can be concluded that there is no further enhancement in the WGS and reforming reactions with increased Ni loading. Generally, increasing the metal loading could lead to particle agglomeration by a sintering effect on the catalysts surface, thereby reducing catalytic activity. Growth of the Ni particles under SCWG conditions causes a reduction in the number of active sites and leads to intense catalyst deactivation [42]. This phenomenon can be seen in the poor catalyst performances in terms of similar hydrogen yield and carbon gasification, even with increased Ni loading. Besides, the presence of overlapping peaks at 700 °C in the TPR profile with Ni addition indicates possible particle agglomeration on the catalysts. Generally, highly dispersed, smaller-sized Ni particles tend to form very strong bonds with the support and exhibit a high-temperature reduction peak [27]. However, the formation of larger Ni particles could cause a shift in the reduction temperature to the left, in agreement with weak interactions between support added Ni [28]. In addition, such transitions on the catalyst reduction peaks observed in the TPR profiles are caused by the presence of larger Ni particles, which show lower catalytic activity with increasing Ni loading. Furthermore, the production of CO₂, CO, and CH₄ is highly influenced by the presence of metallic catalysts, as they are mainly produced from the degradation of dissolved EFB compounds. Metallic Ni was reported to be very active in C–C bond breaking and in promoting gasification reactions. Table 3 shows the carbon concentration in the gas phase, which shows the ability of the catalysts to promote carbon conversion. The carbon concentration increased slightly after 5–8 wt% Ni addition, but then dropped with further increase, due to possible particle agglomeration phenomena, as described above. Furthermore, the 8% Ni-doped catalyst shows the highest production of CO₂, CO, and CH₄, which are mainly produced from functional group cleavages and

Table 3 Carbon concentration in the gas phase with increasing reaction time

Reaction time (min)	Carbon concentration in gas phase (mmol mL ⁻¹)			
	8	16	24	32
5ZnO/5Ni–CaO	16.3	16.3	17.1	16.3
10ZnO/5Ni–CaO	18.1	16.7	16.7	17.0
15ZnO/5Ni–CaO	17.0	15.1	14.2	16.6
5ZnO/8Ni–CaO	20.3	–	–	–
5ZnO/10Ni–CaO	16.8	–	–	–
5ZnO/12Ni–CaO	16.0	–	–	–
5ZnO/15Ni–CaO	16.0	–	–	–

Fig. 7 Effect of Ni loading on 5 wt% ZnO-doped CaO catalysts



rapturing dissolved liquid oxygenates from EFBs. Among the gases produced, the amount of CO shows a significant difference with the added catalysts, whereby the production increased with up to 8 wt% Ni loading and dropped with further increase. However, based on the H₂ concentration obtained, it can be concluded that changes in the amount of CO were not fully influenced by the WGS reaction, where there was no increase in the amount of H₂ produced with CO reduction. Thus, a lower tendency for functional group cleavages and reduced C–C bond rupture are favored at higher Ni loadings. A loading of 5–8 wt% Ni was found to be adequate with 5 wt% ZnO loading on CaO catalysts, which improved hydrogen production through WGS and reforming reactions.

Conclusion

This investigation shows the optimum formulation of CaO-based catalysts with the addition of ZnO and Ni. Increasing the ZnO loading from 5 to 15 wt% does not show a notable improvement in terms of hydrogen production. In fact, 10 and 15 wt% ZnO-doped catalysts led to a decrease in hydrogen production. In addition, a Ni loading above 8 wt% reduced the catalytic activity because of particle agglomeration. Thus, a loading of 5–8% Ni was found to be appropriate to catalyze C–C bond breaking, as indicated by the higher carbon concentration in the product gas. Thus, among the prepared catalysts, 5 wt% ZnO with a Ni loading of 5 wt% on CaO was found to be the best catalyst, based on the highest hydrogen production and feedstock gasification. The synergetic effects of the Ni₈Zn₂O phase in the CaO catalyst significantly promote the water gas shift reaction and elevate the overall gas production. Besides, reaction time shows no further improvement in term of carbon conversion as a result of

thermally stable tarry compounds formation. However, the gas composition changed, due to various reaction mechanisms progressing simultaneously, including the WGS and methanation reactions. Hydrogen projected an increasing trend over time, boost by a progressing WGS reaction, as indicated by the decreasing amount of CO. In addition, the CH₄ concentration was found to increase over time, which was caused by both functional group cleavage and the methanation reaction aided by the presence of metallic Ni catalysts. Thus, the addition of ZnO and Ni to an appropriate amount of CaO produced an effective catalyst that shows high selectivity for hydrogen production through an enhanced WGS reaction.

Funding information The authors express great appreciation to financial support from the Ministry of Higher Education of Long Term Research Grant Scheme (LRSG) NanoMITE (vot no. 5526308) and Universiti Putra Malaysia.

References

- Rodriguez Correa C, Kruse A (2018) Supercritical water gasification of biomass for hydrogen production-review. *J Supercrit Fluids* 133:573–590
- Phang KY, Lau SW (2017) A survey on the usage of biomass wastes from palm oil mills on sustainable development of oil palm plantations in Sarawak. *IOP Conf Ser: Mater Sci Eng* 206:012091. <https://doi.org/10.1088/1757-899X/206/1/012091>
- Agensi Inovasi Malaysia (2013) National Biomass Strategy 2020: new wealth creation for Malaysia's biomass industry; AIM: Selangor, Malaysia
- Matsumura Y, Minowa T, Potic B, Kersten SRA, Prins W, van Swaaij WPM, de Beld BV, Elliott DC, Neuenchwander GG, Kruse A, Antal MJ Jr (2005) Biomass gasification in near- and super-critical water: status and prospects. *Biomass Bioenergy* 29: 269–292

5. Watanabe M, Inomata H, Osada M, Sato T, Adschiri T, Arai K (2003) Catalytic effects of NaOH and ZrO₂ for partial oxidative gasification of n-hexadecane and lignin in supercritical water. *Fuel* 82(5):545–552
6. Wang J, Takarada T (2001) Role of calcium hydroxide in supercritical water gasification of low-rank coal. *Energy Fuel* 15(2):356–362
7. Schmieder H, Abeln J, Boukis N, Dinjus E, Kruse A, Kluth M, Petrich G, Sadri E, Schacht M (2000) Hydrothermal gasification of biomass and organic wastes. *J Supercrit Fluids* 17(2):145–153
8. Kruse A, Faquir M (2007) Hydrothermal biomass gasification – effects of salts, backmixing, and their interaction. *Chem Eng Technol* 30(6):749–754
9. Xu D, Wang S, Hu X, Chen C, Zhang Q, Gong Y (2009) Catalytic gasification of glycine and glycerol in supercritical water. *Int J Hydrogen Energy* 34:5357–5364
10. Guo Y, Wang SZ, Xu DH, Gong YH, Ma HH, Tang XY (2010) Review of catalytic supercritical water gasification for hydrogen production from biomass. *Renew Sust Energy Rev* 14(1):334–343
11. Azadi P, Farhood R (2011) Review of heterogeneous catalyst for sub- and supercritical water gasification of biomass and wastes. *Int J Hydrogen Energy* 36:9529–9541
12. Xu X, Matsumura Y, Stenberg J, Antal MJJ (1996) Carbon-catalyzed gasification of organic feedstocks in supercritical water. *Ind Eng Chem Res* 35(8):2522–2530
13. Yamaguchi A, Hiyoshi N, Sato O, Bando KK, Osada M, Shirai M (2009) Hydrogen production from woody biomass over supported metal catalysts in supercritical water. *Catal Today* 146(6):192–195
14. Azadi P, Afif E, Azadi F, Farnood R (2012) Screening of nickel catalyst for selective hydrogen production using supercritical water gasification of glucose. *Green Chem* 14:1766–1777
15. Osada M, Sato O, Arai K, Shirai M (2006) Stability of supported ruthenium catalysts for lignin gasification in supercritical water. *Energy Fuel* 20(6):2337–2343
16. Cao C, Zhang Y, Cao W, Jin H, Guo L, Huo Z (2017) Transition metal oxides as catalysts for hydrogen production from supercritical water gasification of glucose. *Catal Lett* 147:828–836
17. Zhang R, Jiang W, Cheng L, Sun B, Sun D, Bi J (2010) Hydrogen production from lignite via supercritical water in flow-type reactor. *Int J Hydrogen Energy* 35(21):11810–11815
18. Xia WX, Hou YH, Chang G, Weng WZ, Han GB, Wan HL (2012) Partial oxidation of methane into syngas (H₂ + CO) over effective high-dispersed Ni/SiO₂ catalysts synthesized by a sol–gel method. *Int J Hydrogen Energy* 37:8343–8353
19. Gaskell KJ, Starace A, Langell MA (2007) Zn_xNi_{1-x}O rocksalt oxide surfaces: novel environment for Zn²⁺ and its effect on the NiO band structure. *J Phys Chem C* 111:13912–13921
20. Taufiq-Yap YH, Sivasangar S, Salmiaton A (2012) Enhancement of hydrogen production by secondary metal oxide dopants on NiO/CaO material for catalytic gasification of empty palm fruit bunches. *Energy* 47:158–165
21. Garcia V, Fernandez JJ, Ruiz W, Mondragon F, Moreno A (2009) Effect of MgO addition on the basicity of Ni/ZrO₂ and on its catalytic activity in carbon dioxide reforming of methane. *Catal Commun* 11(4):240–246
22. Taufiq-Yap YH, Lee HV, Hussein MZ, Yunus RR (2011) Calcium-based mixed oxide catalysts for methanolysis of *Jatropha curcas* oil to biodiesel. *Biomass Bioenergy* 35:827–834
23. Teo SH, Rashid U, Taufiq-Yap YH (2014) Biodiesel production from crude *Jatropha Curcas* oil using calcium based mixed oxide catalysts. *Fuel* 136:244–252
24. Yan B, Wu J, Xie C, He F, Wei C (2009) Supercritical water gasification with Ni/ZrO₂ catalyst for hydrogen production from model wastewater of polyethylene glycol. *J Supercrit Fluids* 50(2):155–161
25. Tang CW, Chuang SSC (2014) The effect of reduction of pretreated NiO-ZnO catalysts on the water gas shift reaction for hydrogen production as studied by in situ DRIFTS/MS. *Int J Hydrogen Energy* 39(2):788–797
26. Brown R, Cooper ME, Whan DA (1982) Temperature programmed reduction of alumina-supported iron, cobalt and nickel bimetallic catalysts. *Appl Catal* 3:177–186
27. Zhang X, Liu J, Jing Y, Xie Y (2003) Support effects on the catalytic behavior of NiO/Al₂O₃ for oxidative dehydrogenation of ethane to ethylene. *Appl Catal A: Gene* 240(1–2):143–150
28. Li C, Chen YW (1995) Temperature-programmed-reduction studies of nickel oxide/alumina catalysts: effects of the preparation method. *Thermochim Acta* 256(2):457–465
29. Barati M, Babatabar M, Tavasoli A, Dalai AK, Das U (2014) Hydrogen production via supercritical water gasification of bagasse using unpromoted and zinc promoted Ru/γ-Al₂O₃ nano catalysts. *Fuel Process Technol* 123:140–148
30. Sato T, Inada K, Itoh N (2011) Gasification of bean curd refuse with carbon supported noble metal catalysts in supercritical water. *Biomass Bioenergy* 35(3):1245–1251
31. Hao X, Guo L, Zhang X, Guan Y (2005) Hydrogen production from catalytic gasification of cellulose in supercritical water. *Chem Eng J* 110(1–3):57–65
32. Sivasangar S, Mastuli MS, Islam A, Taufiq Yap YH (2015) Screening of modified CaO-based catalysts with a series of dopants for the supercritical water gasification of empty palm fruit bunches to produce hydrogen. *RSC Adv* 5:36798–36808
33. Mastuli MS, Kamarulzaman N, Kasim MF, Sivasangar S, Saiman MI, Taufiq-Yap YH (2017) Catalytic gasification of oil palm frond biomass in supercritical water using MgO supported Ni, Cu and Zn oxides as catalysts for hydrogen production. *Int J Hydrogen Energy* 42:11215–11228
34. Azadi P, Khan S, Strobel F, Azadi F, Farnood R (2012) Hydrogen production from cellulose, lignin, bark and model carbohydrates in supercritical water using nickel and ruthenium catalysts. *Appl Catal B Environ* 117–118:330–338
35. Lee IG (2011) Effect of metal addition to Ni/activated charcoal catalyst on gasification of glucose in supercritical water. *Int J Hydrogen Energy* 36(15):8869–8877
36. Elliott DC, Hallen RT, Sealock LJ Jr (1983) Aqueous catalyst systems for the water-gas shift reaction. 2. Mechanism of basic catalysis. *Ind Eng Chem Prod Res Dev* 22:431–435
37. Xu CC, Donald J (2012) Upgrading peat to gas and liquid fuels in supercritical water with catalysts. *Fuel* 102:16–25
38. Sivasangar S, Zainal Z, Salmiaton A, Taufiq-Yap YH (2015) Supercritical water gasification of empty fruit bunches from oil palm for hydrogen production. *Fuel* 143:563–569
39. Minowa T, Zhen F, Ogi T (1998) Cellulose decomposition in hot-compressed water with alkali or nickel catalyst. *J Supercrit Fluids* 13(1–3):253–259
40. Tiong L, Komiyama M (2019) Supercritical water gasification of microalga *Chlorella vulgaris* over supported Ru. *J Supercrit Fluids* 144:1–7
41. Osada M, Sato T, Watanabe W, Adschiri T, Arai K (2004) Low-temperature catalytic gasification of lignin and cellulose with a ruthenium catalyst in supercritical water. *Energy Fuel* 18:327–333
42. Lu Y, Zhu Y, Li S, Zhang X, Guo L (2014) Behavior of nickel catalysts in supercritical water gasification of glucose: influence of support. *Biomass Bioenergy* 67:125–136